Journal of the Indian Society of Remote Sensing (October 2024) 52(10):2177–2189
https://doi.org/10.1007/s12524-024-01938-7

RESEARCH ARTICLE

Effects of Digital Elevation Models on Spatial Characterisation of Landslides in the Kalka-Shimla Region of the Indian Himalayas

Ankur Sharma[1] · **Har Amrit Singh Sandhu**[1]

Received: 7 June 2022 / Accepted: 21 June 2024 / Published online: 5 July 2024

Abstract

Landslides are complex geohazards responsible for damage to life, the natural environment, and essential infrastructures like buildings, roads, and transmission lines in mountainous regions. The modeling of topographic input parameters for landslide-related investigations is often based on Digital Elevation Models (DEMs), which serve as a crucial geospatial data source. The present study attempts to analyze the effects of DEMs, obtained from different sources and varying in spatial resolution, on terrain feature estimation and spatial characterization of landslide-affected areas in the Indian Himalayas. Carto-DEM version 3R1 and ALOS PALSAR DEM are used to generate two geodatabases of DEM-derived landslide causative factors, each including digital maps of Elevation, Slope, Aspect, Curvature, Terrain Ruggedness Index, and Distance to Drainage. The generated geodatabases are utilized for conducting a spatial frequency distribution analysis to characterize the selected area into spatial bins with similar topographic characteristics. A comparative study of this analysis reveals that both the DEMs exhibited comparable topographic characteristics on a general level. However, considerable variations are observed when both the geodatabases are scrutinized closely. The results of this study highlight that the quality of the DEM used may affect its usability in a specific investigation and hope to add to the scientific discourse on the effects of DEM on landslide-related studies.

Keywords Landslide inventory · Topographical characterization · Spatial frequency distribution analysis · Digital elevation model (DEM) · Landslide zonation mapping · Geographical information system (GIS)

Introduction

Landslides are amongst the most destructive and frequently occurring natural disasters in mountainous terrains (Saha et al., 2002, 2022). They occur due to the movement of rocks, earth, or debris down an unstable slope in the form of slope failure, rockfall, mudflow, and debris flow (Chawla et al., 2018; Cruden, 1991). Their occurrence is controlled by geological and geomorphological processes and mainly depends on the local terrain conditions (El Jazouli et al., 2019). Landslides can occur on unstable slopes due to factors like deforestation, changing hydrological conditions, stream erosion, volcanic eruption, and anthropogenic activity (Dahal et al., 2006; Dai et al., 2002; Glade, 2002; Gorsevski et al., 2006; Keefer, 1984; Pandit et al., 2021; Raghuvanshi et al., 2014; Schuster & Highland, 2007; Tropeano & Turconi, 2002; van Beek & van Asch, 2004). High precipitation and seismicity, in particular, are the two main triggering factors associated with landslides (Chawla et al., 2017; Lin et al., 2017; Niu et al., 2014; Xu et al., 2014).

Landslides inflict extensive damage globally, affecting the natural landscape, causing economic losses, and resulting in human tragedies (Batar et al., 2017; Fell et al., 2008; Geertsema & Pojar, 2007; Kanungo et al., 2006; Meusburger & Alewell, 2008; National Disaster Management Authority, 2019; Promper et al., 2014; Schuster & Fleming, 1986; Schuster & Highland, 2007; Tan et al., 2020). Despite their impact, the development of a reliable, cost-effective, and efficient landslide early warning system is in its early stages (Naidu et al., 2018). Hence, in the case of landslides, zonation maps incorporating technologies like Remote sensing, Geographical Information Systems (GIS), and modern techniques like Machine Learning (ML) and Deep Learning are increasingly employed to prioritize resources in the event of a disaster striking (Chang et al., 2020; Huang et al.,

✉ Ankur Sharma
ankursharma.phdciv20@pec.edu.in

[1] Department of Civil Engineering, Punjab Engineering College, Sector 12, Chandigarh 160012, India

2017, 2020; Park & Kim, 2019; Peethambaran et al., 2019; Pourghasemi et al., 2018).

Several GIS-based methods, such as heuristic, quantitative, physical-based, and process-based approaches are employed in landslide zonation mapping studies (Conforti et al., 2014; Kim et al., 2018; Pradhan & Lee, 2010; Soria et al., 2011; Zare et al., 2013). Digital Elevation Models (DEMs) play a crucial role in such studies by providing a digital representation of the physical terrain. Previous studies have explored the impact of DEMs on geomorphological and landslide-related analyses with studies exploring publicly available DEMs like Advanced Spaceborne Thermal Emission and Reflection—Global DEM (ASTER-GDEM), Shuttle Radar Topography Mission (SRTM-DEM), Advanced Land Observing Satellite (ALOS) AW3D30-DEM (ALOS-3D), ALOS Phased Array type L-band Synthetic Aperture Radar (ALOS PALSAR) DEM, and Carto-DEM Ver. 3R1 (Huang et al., 2017; Kanungo et al., 2006; Peethambaran et al., 2019; Pradhan, 2013; Roy & Saha, 2019).

It is reported that DEMs serve as the fundamental framework for modeling the causative factors that contribute to landslides (Batar & Watanabe, 2021; Naseer et al., 2021). The characteristics of these causative factors, in turn, rely on the spatial resolution of the DEMs used, as reported by researchers (Chow & Hodgson, 2009; Rabby et al., 2020). It has been observed that the different processing techniques can affect DEM quality (Mahalingam & Olsen, 2016). The impact of DEM resampling on terrain feature estimation has been reported in various studies (Chow & Hodgson, 2009; Deng et al., 2007). Studies have also reported the impact of some publicly available DEMs on landslide-specific modeling applications (Sarma et al., 2020). Moreover, the impact of DEM quality on the final accuracy of landslide zonation analyses has also been widely reported (Kamiński, 2020; Rabby et al., 2020). However, the impact of the Carto-DEM Ver. 3R1 and the ALOS PALSAR DEM on geomorphological modeling and terrain feature estimation have not been adequately reported in the literature. While several studies have focussed on the final accuracy of the landslide zonation analysis, limited studies have discussed the impact of different DEMs on terrain feature estimation at landslide locations.

Thus, an attempt has been made to analyze the effects of Carto-DEM Ver. 3R1 (approx. 30 m) and ALOS PALSAR DEM (12.5 m) on the spatial characterization of landslide locations in the present study. The selection of these DEMs is motivated by the distinctions in their acquisition technologies, quality, and spatial resolutions. To achieve the objective of the study, the DEMs are used to prepare two geodatabases consisting of digital maps of six causative factors each, including Elevation, Slope, Aspect, Curvature, Terrain Ruggedness Index (TRI), and Distance to Drainage. Subsequently, terrain feature estimation is performed at the landslide locations by conducting a spatial frequency distribution analysis of the selected causative factors. The study highlights differences in the characterization of landslide locations using the selected DEMs, which are based on different processing techniques. The results of the study may guide future researchers in making informed decisions when performing, analyzing, and correlating the effects of DEMs on the estimation of terrain features at landslide locations. Furthermore, it may contribute to the realization of the Sustainable Development Goal (SDG) 15 and Sendai Disaster Risk Reduction (DRR) global targets (a), (b) and (g), and help future researchers in evaluating potential causative factors when undertaking studies related to landslide susceptibility, hazard, or risk zonation mapping.

Study Area

The majority of the study area lies in the Shimla and Solan districts of Himachal Pradesh and the Ambala district of Haryana in the northern part of India. Geographically, the study area lies between longitude 76°53′0″E to 77°13′30″E and latitudes 30°47′30″N to 31°09′00″N covering a cumulative area of approximately 609.91 km^2 (Fig. 1). Kalka, Parwanoo, Solan, and Shimla are some of the major population centers. The study area is dominated by landslide-inducing factors like steep slopes, the highly dissected nature of the hills, high precipitation, and severe earthquake intensities. The annual average temperature varies between a minimum of 9.8 °C and a maximum of 25.9 °C. The study area receives an annual average rainfall of approximately 1251 mm. Geomorphologically, the area is composed of highly dissected hills with intermontane valleys. Major rock groups present in the study area are phyllite and quartzite of the Jutogh group, diamictite and shale of the Baliana group, shale of the Sirmaur/Dharamshala group, and sandstone and siltstone of the Dagshai and Kasauli group. Loamy mountainous soil is the predominant soil type in the study area. Seismologically, the study area is very active and frequented by many earthquakes. According to seismic zonation maps prepared and published by the Government of India, it lies in seismic zone IV and has an attributed peak ground acceleration value of 0.24 g (Bureau of Indian Standards New Delhi, 2002).

Data and Methodology

Landslide Inventory Map

The landslide inventory is prepared in polygon form using multiple data sources, i.e., Bhukosh, the data dissemination portal of the Geological Survey of India, and interpretation of Google Earth images (Amatya et al., 2019; Batar &

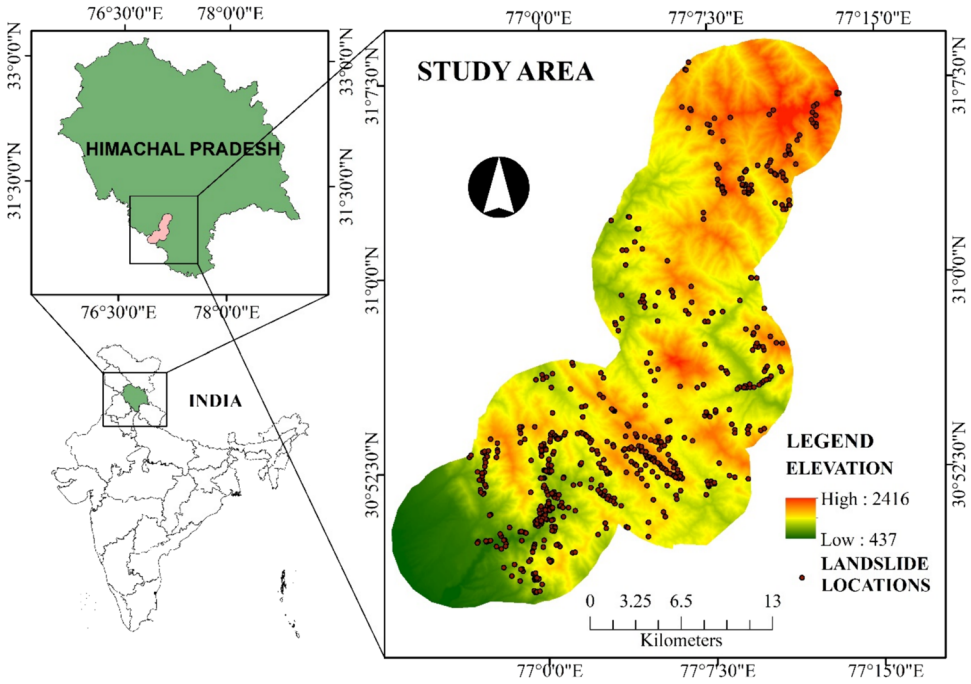

Fig. 1 Location map of the study area and landslide locations

Watanabe, 2021; Hao et al., 2020; Roy & Saha, 2019; Shirzadi et al., 2018). The inventory is then rasterized to match the resolutions of Carto-DEM Ver. 3R1 and ALOS PALSAR DEM. The cumulative area of all the landslide polygons in the original inventory is approximately 647,081 m^2. However, after rasterization, the final areas of the two inventory maps are approximately 655,997 m^2 at the resolution of Carto-DEM Ver. 3R1 and approximately 667,188 m^2 at the resolution of ALOS PALSAR DEM. This difference may be neglected as the total error in the cumulative landslide-affected area in both the inventory maps is only + 1.38% and + 3.10%, respectively. Hence, the prepared inventory maps are used for further analysis.

Landslide Causative Factors

Two geodatabases of DEM-derived landslide causative factors were generated from the selected DEMs, each comprising digital maps of elevation, slope, aspect, curvature, TRI, and distance to drainage, respectively (Figs. 2 and 3). The values of the causative factors were extracted at the landslide locations using raster sampling techniques. Variations were observed between these geodatabases because of the differences in their accuracies, processing technologies, and quality. On analyzing the extracted raster values using the Kruskal–Wallis test, it was seen that the distributions of elevation, slope, aspect, and curvature were statistically the same between the geodatabases while significant differences were observed in the distribution of TRI and distance to drainage. Table 1 presents the results of exploratory data analysis for the two geodatabases used in the study.

The elevation of a place affects factors like the degree of weathering of the slope-forming materials (Pham et al., 2016), the amount of precipitation received at a location, and local temperature, which further affect the stability of the hill slopes. The slope angle of the hill faces is one of the primary factors that can induce instabilities and lead to failures. The slope maps of the study area are derived using surface analysis of the DEMs. The aspect of the hill slopes impacts the landslide occurrences as the slopes facing different directions receive different amounts of rainfall and solar radiation, which may affect the vegetation density. Hence, slopes facing a particular direction may be more prone to landslides (Sarkar et al., 1995, 2013). Curvature is a geomorphological factor that determines the flow of water, thus, affecting landslide occurrences (Ayalew et al., 2004; Tien Bui et al., 2017). In this study, an upward convex surface is depicted as having positive curvature, flat surfaces have no curvature, while an upward concave surface has negative curvature. TRI is used to assess the overall terrain heterogeneity and degree of undulations of the surface features. TRI is defined as the mean absolute difference in elevation between a central pixel and its eight surrounding pixels on a DEM (Riley et al., 1999). The presence of drainage may aggravate the erosional activity on the hill faces due to excessive surface runoff. Hence, slope failures may be associated with the drainage channels (Sarkar & Kanungo, 2004). Therefore, the drainage network of the study area is extracted using watershed analysis of the DEMs. During analysis, the accumulation area is kept constant by proportionately adjusting the number of contributing pixels for both the

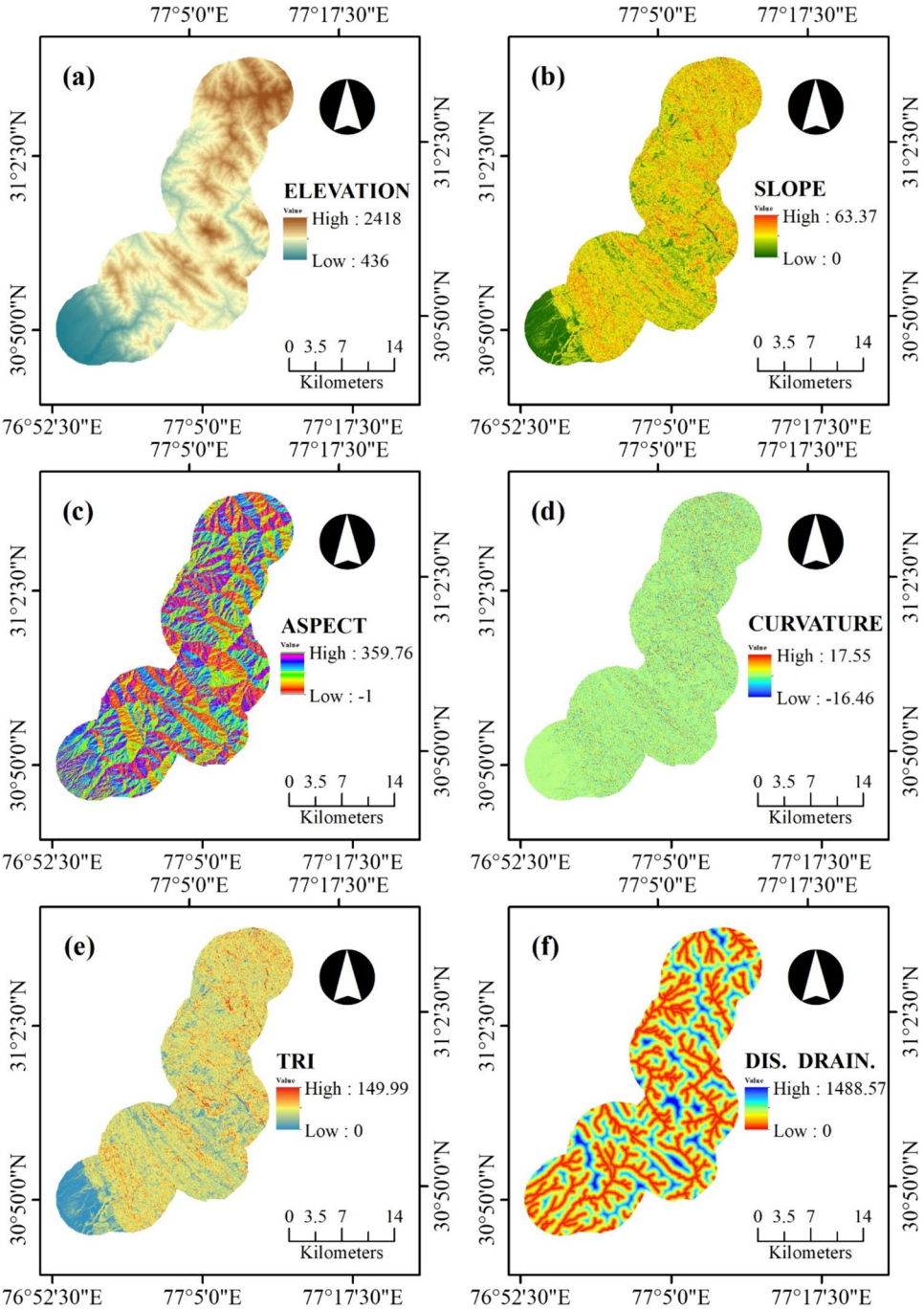

Fig. 2 Thematic maps of the causative factors derived from Carto-DEM Ver. 3R1: **a** Elevation, **b** Slope, **c** Aspect, **d** Curvature, **e** TRI, and **f** Distance to drainage

DEMs. Then, Euclidian distance is calculated from the drainage networks to obtain the distance to drainage maps.

Spatial Frequency Distribution Analysis

After preparing the digital maps for landslide inventory and the landslide causative factors, raster values of all the causative factors are extracted at the landslide locations using raster sampling tools in GIS software and compiled in the form of a tabular worksheet by reclassifying them into different classes. Furthermore, the number of pixels occupying a particular class is converted to a percentage of the total number of pixels representing the cumulative study area. Similarly, the landslide-affected pixels within each class are also converted to a percentage of the cumulative landslide-affected area. Then the impact of the selected DEMs on the spatial characterization of the landslide locations is analyzed in terms of variations in the Landslide Severity Index (LSI) values calculated for all the landslide causative factors (Eq. 1):

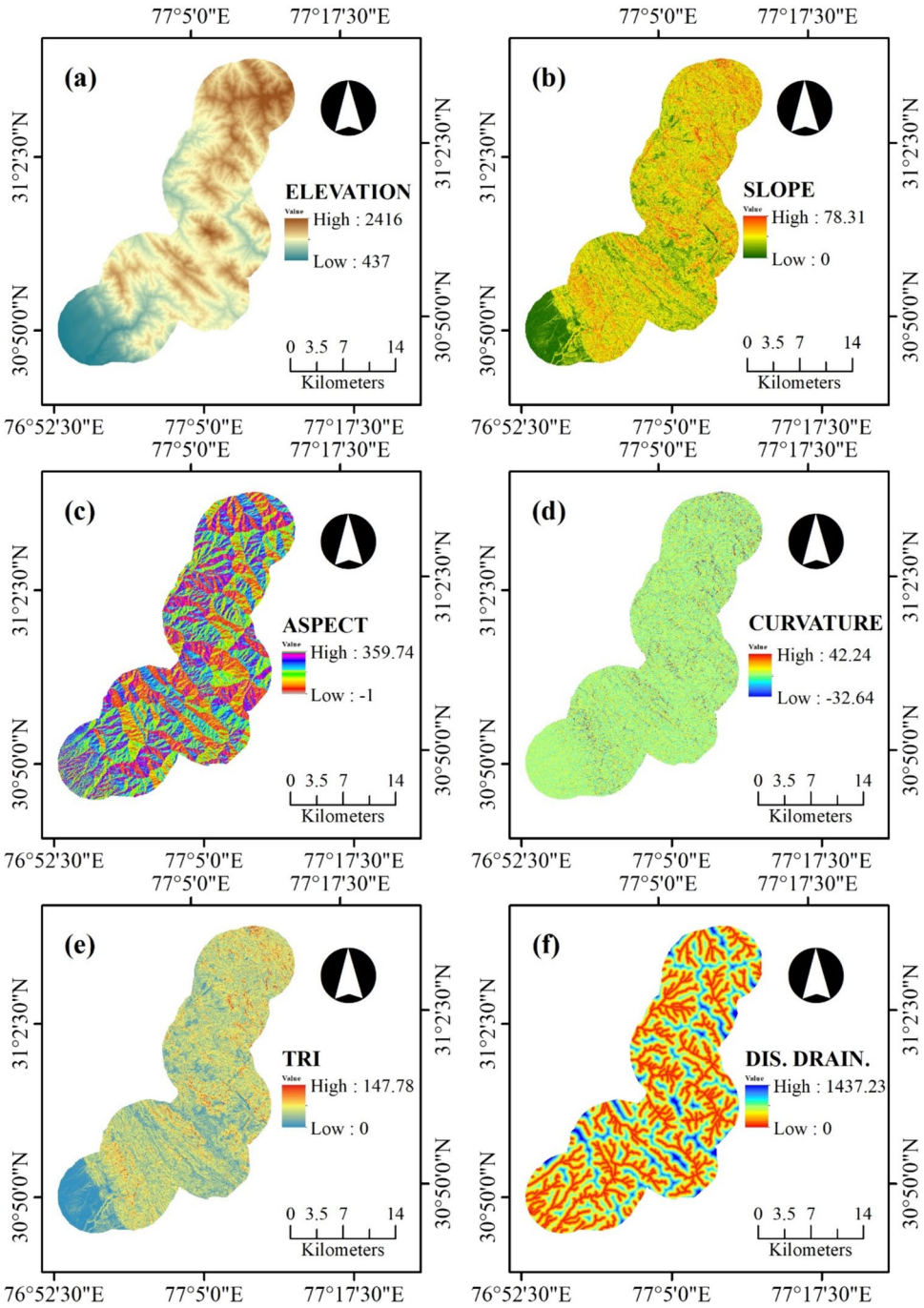

Fig. 3 Thematic maps of the causative factors derived from ALOS PALSAR DEM: **a** Elevation, **b** Slope, **c** Aspect, **d** Curvature, **e** TRI, and **f** Distance to drainage

$$\text{LSI} = \frac{\text{Landslide affected pixels in a class of landslide causative factor(\%)}}{\text{Total number of pixels in a class of landslide causative factor(\%)}} \quad (1)$$

Results

The following sections elaborate on the results of the spatial frequency distribution analysis carried out to determine the impact when Carto-DEM Ver. 3R1 and ALOS PALSAR DEM are used for the terrain feature estimation at the landslide locations. The observations of the varying LSI values are also presented along with these results for both DEMs.

Dataset Derived from Carto-DEM Ver. 3R1

Table 2 summarises the spatial characteristics of the landslide locations based on the analysis conducted using the Carto-DEM Ver. 3R1 geodatabase. The elevation of the

Table 1 Spread of values of the landslide causative factors in the two generated geodatabases

Value	Dataset	Elevation	Slope	Aspect (nominal)	Curvature	TRI	Dist. to drainage
Minimum value	Carto-DEM	436	0.00	–	− 16.46	0.00	0.00
	ALOS PALSAR	437	0.00	–	− 32.64	0.00	0.00
Q1	Carto-DEM	1142	25.63	–	− 1.21	37.74	203.25
	ALOS PALSAR	1142	23.89	–	− 0.64	13.89	179.23
Median	Carto-DEM	1414	30.64	–	0.24	44.89	433.54
	ALOS PALSAR	1426.50	29.90	–	0	17.86	387.33
Q3	Carto-DEM	1643	35.60	–	1.57	53.28	741.78
	ALOS PALSAR	1662	36.38	–	1.28	22.87	621.55
Maximum value	Carto-DEM	2418	63.37	–	17.55	149.99	1488.57
	ALOS PALSAR	2416	78.31	–	42.24	147.78	1437.23
Outliers (%)	Carto-DEM	0.00	1.51	–	1.76	1.89	0.00
	ALOS PALSAR	0.00	1.22	–	1.90	3.21	0.00

study area is divided into nine classes using Jenks natural breaks classification. The results reveal that the maximum landslide-affected area (18.58%) lies between the elevation range of 1598 m and 1758 m, followed by the elevation between 973 and 1166 m (17.77%) and between 1314 and 1452 m (15.33%). However, the LSI is the highest (2.06) at relatively lower elevations between 713 and 973 m followed by the range 973–1166 m (1.65) and 1598–1758 m (1.46). The slope is divided into eight classes using equal intervals classification for ease of comprehension of the results (Zhao & Chen, 2020). It is observed that the majority of the study area (60.39%) has a slope variation between 20° and 40°. Moreover, approximately three-fourths of the landslide-affected area (75.63%) also lies in the same class. LSI is highest (176.34) for the slope class between 60° and 70°, though the fraction of the study area for this class is very small (0.002%). The second and the third highest landslide severity occurs in the slope ranges of 50° to 60° (3.88), followed by 40° to 50° (2.90). The slope aspect is classified into nine classes using equal interval classification starting from 0°, denoting the north direction, and increasing clockwise till 360° to denote the north direction again (Rawat et al., 2015). The slopes that are not oriented in any direction are denoted as flat. The highest percentage of landslides-affected areas have an aspect angle between 180° and 225° (22.49%) followed by the area having an aspect angle between 225° and 270° (19.86%). The third most landslide-affected slopes have aspect angles between 135° and 180° (12.16%). The highest LSI values occur in the aspect range of 180° to 225° (1.49), followed by 225° to 270° (1.28) and 90° to 135° (1.10). In terms of curvature, higher landslide occurrences are observed in areas with positive curvatures (52.49%) as compared to negative curvatures (45.69%). They are the least in the flat areas (1.83%). Similarly, LSI is highest for areas with positive curvatures (1.08), followed by negative curvatures (0.95), and the least (0.56) for flat areas. TRI map is classified into nine classes using Jenks natural breaks classification. The largest proportion of area affected by landslides is in the TRI ranges of 41.95–49.20 m (23.70%), followed by 35.37–41.95 m (19.23%) and 49.2–58.3 m (18.62%). Progressively higher LSI values are observed for higher TRI values, with the maximum LSI occurring between 71.95 to 149.99 m (3.04) followed by 58.3–71.95 m (2.35) and 49.20–58.30 m (1.85). More than half (52.85%) of the landslide-affected locations lie within 450 m of the drainage features. However, LSI is observed to be highest (4.86) in areas located between 1050 and 1200 m from the drainage features.

Dataset Derived from ALOS PALSAR DEM

Table 3 summarises the spatial characterization of landslide locations based on the analysis conducted using ALOS PALSAR geodatabase. Elevation of the study area is categorized into nine classes using a similar approach as previously used. Here, it is observed that the maximum landslide-affected area (18.47%) lies in the elevation range of 1310–1448 m, followed by 1162–1310 m (16.48%), and 1448–1595 m (15.57%). However, LSI is highest (1.94) at relatively lower elevation ranges of 712–970 m followed by 1595–1756 m (1.70) and 970–1162 m (1.57). The slope map is divided into eight classes using equal interval classification (Zhao & Chen, 2020). It is observed that 56.83% of the study area has a slope variation between 20° and 40°, encompassing 71.80% of the landslide-affected area. The maximum percentage of the landslide-affected area was observed in the slope range of 20° to 30° (37.53%) followed by 30° to 40° (34.26%) and 40° to 50° (12.24%). The highest LSI values occur in the slope range between 60° and 70° (8.92), followed by the locations having slope values above 70° (7.06) and the slope range between 50° and 60° (4.14). The highest percentage of landslide-affected areas have aspect angles in

Table 2 Spatial frequency distribution analysis of the landslide locations using the Carto-DEM geodatabase

Sl. no	Thematic Layer	Classes	Pixels within a class (%) ($\mathbf{A_1}$)	Landslide affected pixels (%) ($\mathbf{B_1}$)	LSI ($\mathbf{C_1}$)
1	Elevation	436–713 m	8.81	1.42	0.16
		713–973 m	4.43	9.14	2.06
		973–1166 m	10.74	17.77	1.65
		1166–1314 m	16.61	10.25	0.62
		1314–1452 m	18.42	15.33	0.83
		1452–1598 m	**15.37**	**14.21**	**0.93**
		1598–1758 m	12.75	18.58	1.46
		1758–1957 m	9.08	10.46	1.15
		1957–2418 m	3.78	2.84	0.75
2	Slope	0°–10°	12. 5	1.42	0.11
		10°–20°	23.62	12.28	0.52
		20°–30°	37.34	34.72	0.93
		30°–40°	**23.05**	**40.91**	1.77
		40°–50°	3.36	9.75	2.90
		50°–60°	0.13	0.51	3.88
		60°–70°	0.00	0.41	**176.34**
		> 70°	0.00	0.00	0.00
3	Aspect	Flat	0.02	0.00	0.00
		0°–45°	12.05	8.61	0.71
		45°–90°	**11.86**	10.33	0.87
		90°–135°	10.01	11.04	1.10
		135°–180°	11.42	12.16	1.06
		180°–225°	15.10	22.49	1.49
		225°–270°	15.52	**19.86**	**1.28**
		270°–315°	13.60	8.21	0.60
		315°–360°	10.43	7.29	0.70
4	Curvature	Negative	48.16	45.69	0.95
		Flat	**3.25**	**1.83**	**0.56**
		Positive	48.59	52.49	1.08
5	TRI	0–12.04 m	7.62	0.10	0.01
		12.04–21.31 m	**9.81**	2.64	0.27
		21.31–28.72 m	14.87	7.83	0.53
		28.72–35.37 m	17.96	**12.61**	0.70
		35.37–41.95 m	18.22	19.23	1.06
		41.95–49.20 m	15.34	23.70	1.55
		49.20–58.30 m	10.06	18.61	1.85
		58.30–71.95 m	4.86	11.39	2.35
		71.95–149.99 m	1.27	3.87	**3.04**
6	Distance to drainage	0–150 m	22.99	18.70	0.81
		150—300 m	**18.62**	18.09	0.97
		300–450 m	17.27	16.06	0.93
		450–600 m	14.24	12.20	0.86
		600–750 m	12.06	13.31	1.10
		750–900 m	8.27	9.86	1.19
		900–1050 m	4.48	3.25	**0.73**
		1050–1200 m	1.63	**7.93**	4.86
		> 1200 m	0.44	0.61	1.34

The bold value indicate the values used to calculate the maximum absolute differences

Table 3 Spatial frequency distribution analysis of the landslide locations using the ALOS PALSAR geodatabase

Sl. No	Thematic Layer	Classes	Pixels within a class (%) ($\mathbf{A_2}$)	Landslide affected pixels (%) ($\mathbf{B_2}$)	LSI ($\mathbf{C_2}$)
1	Elevation	437–712 m	8.80	1.59	0.18
		712–970 m	4.35	8.44	1.94
		970–1162 m	10.61	16.69	1.57
		1162–1310 m	16.48	10.29	0.62
		1310–1448 m	18.47	15.68	0.85
		1448–1595 m	**15.57**	**10.39**	**0.67**
		1595–1756 m	12.88	21.90	1.70
		1756–1954 m	9.03	12.41	1.37
		1954–2416 m	3.82	2.62	0.69
2	Slope	0°–10°	12.68	1.20	0.09
		10°–20°	12.30	11.57	0.46
		20°–30°	36.01	37.53	1.04
		30°–40°	**20.83**	**34.26**	1.65
		40°–50°	4.52	12.24	2.71
		50°–60°	0.57	2.36	4.14
		60°–70°	0.09	0.79	**8.92**
		> 70°	0.01	0.05	7.06
3	Aspect	Flat	0.24	0.00	0.00
		0°–45°	12.85	8.66	0.67
		45°–90°	**10.87**	9.79	0.90
		90°–135°	10.11	11.18	1.11
		135°–180°	11.86	13.37	1.13
		180°–225°	16.08	24.72	1.54
		225°–270°	14.87	**15.68**	**1.05**
		270°–315°	12.67	9.02	0.71
		315°–360°	10.45	7.60	0.73
4	Curvature	Negative	40.73	38.09	0.94
		Flat	**18.62**	**16.06**	**0.86**
		Positive	40.65	45.85	1.13
5	TRI	0–5.39 m	11.16	0.79	0.07
		5.39–9.43 m	**15.92**	4.81	0.30
		9.43–12.92 m	19.60	13.56	0.69
		12.92–16.37 m	19.77	**20.51**	1.04
		16.37–20.15 m	16.37	22.91	1.40
		20.15–24.86 m	10.72	19.26	1.80
		24.86–32.08 m	4.96	11.52	2.32
		32.08–47.92 m	1.34	5.27	3.94
		47.92–147.78 m	0.17	1.37	**8.02**
6	Distance to drainage	0–150 m	27.10	19.50	0.72
		150–300 m	**23.06**	22.55	0.98
		300–450 m	19.20	13.58	0.71
		450–600 m	14.91	16.23	1.09
		600–750 m	9.48	13.68	1.44
		750–900 m	4.59	9.35	2.04
		900–1050 m	1.36	4.33	**3.19**
		1050–1200 m	0.27	**0.77**	2.86
		> 1200 m	0.04	0.00	0.00

The bold value indicate the values used to calculate the maximum absolute differences

the range of 180° to 225° (24.72%) followed by 225° to 270° (15.68%) and 135° to 180° (13.37%). The highest LSI value occurs at locations with aspect angles between 180° and 225° (1.54), while the second and third highest LSI values arise in the aspect ranges between 135° and 180° (1.13) and between 90° and 135° (1.11), respectively. In terms of curvature, 45.85% of the landslides occur in areas with positive curvatures, 38.09% occur in areas with negative curvatures, and 16.06% occur in flat areas. LSI value is highest on slopes with positive curvatures (1.13), followed by the slopes with negative curvatures (0.94), and the least for areas that are flat (0.86). As done for the Carto-DEM geodatabase, the study area is divided into nine TRI classes, with most of the study area having TRI values between 0 and 24.86 m (93.53%). The highest LSI value occurs in the TRI range of 47.92–147.78 (8.02), followed by 32.08–47.92 m (3.94) and 24.86–32.08 m (2.32). In terms of the distance to drainage, 55.64% of the landslide locations lie within 450 m of the drainage features. The highest LSI value is observed at a distance between 900 to 1050 m (3.19), followed by 1050–1200 m (2.86) and 750–900 m (2.04) from the drainage features.

Discussions

DEM provides the fundamental framework for terrain feature estimation and modeling for landslide-related analyses using Remote Sensing and GIS tools. DEM-derived parameters are often used as input factors for modeling geomorphological conditions in landslide susceptibility, hazard, and risk zonation mapping studies. It is reported that the source and resolution of the DEMs used in such studies influence the prediction accuracy of the employed models (Chow & Hodgson, 2009; Deng et al., 2007). This influence is mostly attributed to the impact of variations in the DEM-derived parameters on the results of the simulation (Sarma et al., 2020). The present study analyzes this impact using two geodatabases of DEM-derived landslide causative factors generated using Carto-DEM Ver. 3R1, which is based on a photogrammetric approach that extracts the elevation data from stereo images, and ALOS PALSAR DEM, which is generated using SAR technology. The variations in terrain feature estimation resulting from these two DEMs are highlighted by conducting a comparative study of the spatial frequency distribution analysis of the landslide locations. Table 4 summarizes these variations in the form of absolute maximum differences observed during the analysis of the two geodatabases for each of the causative factors. The variations are reported as percentages by taking the ALOS PALSAR geodatabase as a reference, as it has a finer resolution.

The findings show a difference in the evaluated landslide severity between the two geodatabases for elevation, as measured by the highest LSI values. Comparing the two geodatabases, it is observed that the greatest LSI value is marginally lower, and the second and third highest LSI values are marginally higher (Tables 2 and 3) in the Carto-DEM geodatabase. Most landslides occurred in moderate-sloped regions characterized by slope gradients between 20° and 40° in both the geodatabases. Such observations are interesting because it is intuitive to think that landslide activity should be elevated in areas characterized by higher slope gradients. However, similar observations have been reported in other studies in different parts of the world where landslides occur in regions characterized by low to moderate slope gradients (Naseer et al., 2021; Xu et al., 2014). This is because of the distribution of the slope-forming materials where steeper slopes are usually composed of rocky materials that effectively transfer all their weight to the toe of the slope. Approximately two-fifths of the landslide-affected areas exhibited an aspect angle between 180° and 270°, although the distribution of these areas between the intervals 180°–225° and 225°–270° varied between both the geodatabases. Similar observations are also reported in other studies of the Indian Himalayan region, which report that slopes oriented in the south-southwestern direction are more prone to landslides (Sarkar et al., 2013).

Significant variations were observed in the characterization of the study area for all the causative factors, with the maximum variation being observed for curvature (Table 4). Also, the landslide occurrences in flat terrain were found to be significantly more prominent (8.79 times) in the ALOS PALSAR geodatabase. In both the geodatabases, progressively higher LSI values were observed at locations with

Table 4 Absolute maximum differences (%) between corresponding values of landslide causative factors from the two geodatabases used in this study for (1) percentage of the study area (2) percentage of landslide affected area (3) LSI values in a particular variable class

Sr. no	Thematic layer	Max $\lvert (A_1 - A_2) \rvert$ (%)	Max $\lvert (B_1 - B_2) \rvert$ (%)	Max $\lvert (C_1 - C_2) \rvert$ (%)
1	Elevation	1.30	36.83	38.63
2	Slope	10.69	19.41	1876.75
3	Aspect	9.03	26.67	21.35
4	Curvature	82.55	88.62	34.81
5	TRI	38.39	38.50	62.04
6	Distance to drainage	19.26	930.24	77.25

higher values of TRI, which is logical because the higher values of TRI indicate that the locations have a higher elevation difference from the surrounding locations. Furthermore, more than half of the landslides occurred within 450 m of the drainage features for both geodatabases. The literature supports similar observations of landslides occurring near drainage features (Chawla et al., 2019; Sarkar & Kanungo, 2004). However, the greatest LSI values are observed farther away from the drainage features for both the geodatabases, in contradiction to the general observations by other researchers (Asmare, 2023; Jones et al., 2021). Moreover, as compared to the observations from the Carto-DEM geodatabase, the areas of higher LSIs were situated relatively nearer to the drainage features in the ALOS PALSAR geodatabase. On further investigation employing the interpretation of remotely sensed satellite images, it was concluded that higher LSI values farther from the drainage features may have resulted from anthropogenic activities in the form of residential construction and other infrastructure development. The variations in the estimated distances from drainage features of these high LSI values were attributed to the effects of the two DEMs on the characterization of the landslide regions.

Conclusions

The accuracy of a DEM in representing the topographical characteristics of a given location is crucial for landslide-related studies. In particular, the accuracy of the results in such analyses is significantly influenced by the variations in the DEM-derived parameters. Thus, this study investigated the variations in the spatial characterization of landslide locations, employing Carto-DEM Ver. 3R1 and ALOS PALSAR DEM. Differences were observed in terrain feature estimation by conducting spatial frequency distribution analyses of the geodatabases generated from these DEMs. The results of the analyses reveal substantial variations between the two geodatabases employed.

Though both DEMs exhibited comparable topographical features, discrepancies were observed upon closer scrutiny. Although the derived causative factors from both the selected DEMs successfully captured the general characteristics of the landslide locations, the distribution of landslide-affected areas varied significantly. A comparative analysis of the generated geodatabases showed that the slope gradients in the Carto-DEM geodatabase between 20° and 30° varied by + 7.45% and 30°–40° varied by − 19.41%, respectively as compared to the ALOS PALSAR geodatabase. A notable difference was observed in the landslide areas with flat terrain, primarily because of the difference in the resolutions of the two DEMs. Terrain ruggedness and drainage features were captured fairly well by both the DEMs with progressively higher values of LSI being observed for increasing TRI values. A comparative analysis of the LSI values revealed significant differences in terms of slope, with the Carto-DEM exhibiting LSI values over 18 times larger than the ALOS PALSAR DEM.

The results of this study suggest that the source and resolution of the selected DEMs may influence terrain feature estimation, thus affecting their usability in landslide-related studies. The choice of a suitable DEM for terrain modeling and surface feature estimation may be impacted by the availability of data. However, the choice greatly depends upon the specific setting of the investigation, and it is crucial to acknowledge that topographic characteristics exhibit considerable variation across diverse landscapes. Consequently, the selection of an appropriate DEM depends upon the objectives of the research, the characteristics of the study location, and a comprehensive assessment of the employed models.

Acknowledgements The authors would like to sincerely thank the anonymous reviewers and members of the editorial team for their comments and contributions.

Author's Contribution AS Conceptualisation, Methodology, Software, Validation, Formal analysis, Investigation, Data curation, Writing—Original Draft. HASS Supervision, Writing—Reviewing and editing.

Funding The authors declare that no funds, grants, or other support were received during the preparation of this manuscript.

Declarations:

Conflict of interest The authors declared that they have no conflict of interest.

Data Availability The data that support the findings of this study are available from the corresponding author, Ankur Sharma, upon reasonable request.

References

Amatya, P., Kirschbaum, D., & Stanley, T. (2019). Use of very high-resolution optical data for landslide mapping and susceptibility analysis along the Karnali highway, Nepal. *Remote Sensing*. https://doi.org/10.3390/rs11192284

Asmare, D. (2023). Application and validation of AHP and FR methods for landslide susceptibility mapping around choke mountain, Northwestern, Ethiopia. *Scientific African*. https://doi.org/10.1016/j.sciaf.2022.e01470

Ayalew, L., Yamagishi, H., & Ugawa, N. (2004). Landslide susceptibility mapping using GIS-based weighted linear combination, the case in Tsugawa area of Agano River, Niigata Prefecture, Japan. *Landslides, 1*(1), 73–81. https://doi.org/10.1007/s10346-003-0006-9

Batar, A. K., & Watanabe, T. (2021). Landslide susceptibility mapping and assessment using geospatial platforms and weights of evidence (WoE) method in the Indian Himalayan region: Recent

developments, gaps, and future directions. *ISPRS International Journal of Geo-Information,*. https://doi.org/10.3390/ijgi10030114

Batar, A. K., Watanabe, T., & Kumar, A.(2017). Assessment of land-use/land-cover change and forest fragmentation in the Garhwal Himalayan region of India. *Environments—MDPI, 4*(2), 1–16. https://doi.org/10.3390/environments4020034

Bureau of Indian Standards New Delhi. (2002). Criteria for earthquake resistant design of structures—general provisions and buildings part-1. *Bureau of Indian Standards, New Delhi, Part, 1*, 1–39.

Chawla, A., Chawla, S., Pasupuleti, S., Rao, A. C. S., Sarkar, K., & Dwivedi, R. Landslide susceptibility mapping in Darjeeling Himalayas, India. *Advances in Civil Engineering*. https://doi.org/10.1155/2018/6416492

Chawla, A., Pasupuleti, S., Chawla, S., Rao, A. C. S., Sarkar, K., & Dwivedi, R. (2019). Landslide susceptibility zonation mapping: A Case study from Darjeeling District, Eastern Himalayas, India. *Journal of the Indian Society of Remote Sensing, 47*(3), 497–511. https://doi.org/10.1007/s12524-018-0916-6

Chawla, S., Chawla, A., & Pasupuleti, S.(2017). A feasible approach for landslide susceptibility map using GIS 101–110. https://doi.org/10.1061/9780784480717.010

Chang, Z., Du, Z., Zhang, F., Huang, F., Chen, J., Li, W., & Guo, Z. (2020). Landslide susceptibility prediction based on remote sensing images and GIS: Comparisons of supervised and unsupervised machine learning models. *Remote Sensing*. https://doi.org/10.3390/rs12030502

Chow, T. E., & Hodgson, M. E. (2009). Effects of lidar post-spacing and DEM resolution to mean slope estimation. *International Journal of Geographical Information Science, 23*(10), 1277–1295. https://doi.org/10.1080/13658810802344127

Conforti, M., Pascale, S., Robustelli, G., & Sdao, F. (2014). Evaluation of prediction capability of the artificial neural networks for mapping landslide susceptibility in the Turbolo River catchment (northern Calabria, Italy). *CATENA, 113*, 236–250. https://doi.org/10.1016/j.catena.2013.08.006

Cruden, D. M. (1991). A simple definition of a landslide. *Bulletin of the International Association of Engineering Geology-Bulletin De L'association Internationale De Géologie De L'ingénieur, 43*(1), 27–29. https://doi.org/10.1007/BF02590167

Dahal, R. K., Hasegawa, S., Masuda, T., & Yamanaka, M. (2006). Roadside Slope Failures in Nepal during Torrential Rainfall and their Mitigation Road construction practice in Nepal. In *Proceedings of the Interpaevent international symposium on Niijigata 2006, disaster mitigation of debris flow, slope failures and landslides* (pp. 503–514).

Dai, F. C., Lee, C. F., & Ngai, Y. Y. (2002). Landslide risk assessment and management: An overview. *Engineering Geology, 64*(1), 65–87. https://doi.org/10.1016/S0013-7952(01)00093-X

Deng, Y., Wilson, J. P., & Bauer, B. O. (2007). DEM resolution dependencies of terrain attributes across a landscape. *International Journal of Geographical Information Science, 21*(2), 187–213. https://doi.org/10.1080/13658810600894364

El Jazouli, A., Barakat, A., & Khellouk, R. (2019). GIS-multicriteria evaluation using AHP for landslide susceptibility mapping in Oum Er Rbia high basin (Morocco). *Geoenvironmental Disasters*. https://doi.org/10.1186/s40677-019-0119-7

Fell, R., Corominas, J., Bonnard, C., Cascini, L., Leroi, E., & Savage, W. Z. (2008). Guidelines for landslide susceptibility, hazard and risk zoning for land use planning. *Engineering Geology, 102*(3–4), 85–98. https://doi.org/10.1016/j.enggeo.2008.03.022

Geertsema, M., & Pojar, J. J. (2007). Influence of landslides on biophysical diversity—A perspective from British Columbia. *Geomorphology, 89*(1–2 SPEC. ISS), 55–69. https://doi.org/10.1016/j.geomorph.2006.07.019

Glade, T. (2002). Landslide occurrence as a response to land use change: A review of evidence from New Zealand. *CATENA, 51*, 297–314.

Gorsevski, P. V., Gessler, P. E., Foltz, R. B., & Elliot, W. J. (2006). Spatial prediction of landslide hazard using logistic regression and ROC analysis. *Transactions in GIS, 10*(3), 395–415. https://doi.org/10.1111/j.1467-9671.2006.01004.x

Hao, L., A., R., Van Westen, C., K. S., S., Ranjan Martha, T., Jaiswal, P., & G. McAdoo, B. (2020). 'Constructing a complete landslide inventory dataset for the 2018 monsoon disaster in Kerala, India, for land use change analysis. *Earth System Science Data, 12*(4), 2899–2918. https://doi.org/10.5194/essd-12-2899-2020

Huang, F., Yin, K., Huang, J., Gui, L., & Wang, P. (2017). Landslide susceptibility mapping based on self-organizing-map network and extreme learning machine. *Engineering Geology, 223*, 11–22. https://doi.org/10.1016/j.enggeo.2017.04.013

Huang, F., Cao, Z., Guo, J., Jiang, S. H., Li, S., & Guo, Z. (2020). Comparisons of heuristic, general statistical and machine learning models for landslide susceptibility prediction and mapping. *CATENA*. https://doi.org/10.1016/j.catena.2020.104580

Jones, S., Kasthurba, A. K., Bhagyanathan, A., & Binoy, B. V. (2021). Landslide susceptibility investigation for Idukki district of Kerala using regression analysis and machine learning. *Arabian Journal of Geosciences*. https://doi.org/10.1007/s12517-021-07156-6

Kamiński, M. (2020). The impact of quality of digital elevation models on the result of landslide susceptibility modeling using the method of weights of evidence. *Geosciences (switzerland), 10*, 1–21. https://doi.org/10.3390/geosciences10120488

Kanungo, D. P., Arora, M. K., Sarkar, S., & Gupta, R. P. (2006). A comparative study of conventional, ANN black box, fuzzy and combined neural and fuzzy weighting procedures for landslide susceptibility zonation in Darjeeling Himalayas. *Engineering Geology, 85*(3–4), 347–366. https://doi.org/10.1016/j.enggeo.2006.03.004

Keefer, D. K. (1984). Landslides caused by earthquakes. *Geological Society of America Bulletin, 95*(4), 406–421. http://pubs.er.usgs.gov/publication/70014049

Kim, J. C., Lee, S., Jung, H. S., & Lee, S. (2018). Landslide susceptibility mapping using random forest and boosted tree models in Pyeong-Chang, Korea. *Geocarto International, 33*(9), 1000–1015. https://doi.org/10.1080/10106049.2017.1323964

Lin, G. F., Chang, M. J., Huang, Y. C., & Ho, J. Y. (2017). Assessment of susceptibility to rainfall-induced landslides using improved self-organizing linear output map, support vector machine, and logistic regression. *Engineering Geology, 224*, 62–74. https://doi.org/10.1016/j.enggeo.2017.05.009

Mahalingam, R., & Olsen, M. J. (2016). Evaluation of the influence of source and spatial resolution of DEMs on derivative products used in landslide mapping. *Geomatics, Natural Hazards and Risk, 7*(6), 1835–1855. https://doi.org/10.1080/19475705.2015.1115431

Meusburger, K., & Alewell, C. (2008). Impacts of anthropogenic and environmental factors on the occurrence of shallow landslides in an alpine catchment (Urseren Valley, Switzerland). *Natural Hazards and Earth System Science, 8*(3), 509–520. https://doi.org/10.5194/nhess-8-509-2008

Naidu, S., Sajinkumar, K. S., Oommen, T., Anuja, V. J., Samuel, R. A., & Muraleedharan, C. (2018). Early warning system for shallow landslides using rainfall threshold and slope stability analysis. *Geoscience Frontiers, 9*(6), 1871–1882. https://doi.org/10.1016/j.gsf.2017.10.008

Naseer, S., Haq, T. U., Khan, A., Tanoli, J. I., Khan, N. G., Qaiser, F. ur R., & Shah, S. T. H. (2021). GIS-based spatial landslide distribution analysis of district Neelum, AJ&K, Pakistan. *Natural Hazards, 106*(1), 965–989. https://doi.org/10.1007/s11069-021-04502-5

National Disaster Management Authority (2019) *A publication of the National DisasterManagement Authority, Government of India*.

Niu, R., Wu, X., Yao, D., Peng, L., Ai, L., & Peng, J. (2014). Susceptibility assessment of landslides triggered by the Lushan earthquake, April 20, 2013, China. *IEEE Journal of Selected Topics in Applied Earth Observations and Remote Sensing, 7*(9), 3979–3992. https://doi.org/10.1109/JSTARS.2014.2308553

Pandit, K., Singh, M., Sharma, S., Sandhu, H. A. S., & Sahoo, J. P. (2021). Back-analysis of a debris slope through numerical methods and field observations of slope displacements. *Indian Geotechnical Journal, 51*(4), 811–828. https://doi.org/10.1007/s40098-021-00553-4

Park, S., & Kim, J. (2019). Landslide susceptibility mapping based on random forest and boosted regression tree models, and a comparison of their performance. *Applied Sciences (switzerland)*. https://doi.org/10.3390/app9050942

Peethambaran, B., Anbalagan, R., Shihabudheen, K. V., & Goswami, A. (2019). Robustness evaluation of fuzzy expert system and extreme learning machine for geographic information system-based landslide susceptibility zonation: A case study from Indian Himalaya. *Environmental Earth Sciences*. https://doi.org/10.1007/s12665-019-8225-0

Pham, B. T., Tien Bui, D., Prakash, I., & Dholakia, M. B. (2016). Rotation forest fuzzy rule-based classifier ensemble for spatial prediction of landslides using GIS. *Natural Hazards, 83*(1), 97–127. https://doi.org/10.1007/s11069-016-2304-2

Pourghasemi, H. R., Gayen, A., Park, S., Lee, C. W., & Lee, S. (2018). "Assessment of landslide-prone areas and their zonation using logistic regression, LogitBoost, and naïvebayes machine-learning algorithms. *Sustainability (switzerland)*. https://doi.org/10.3390/su10103697

Pradhan, B. (2013). A comparative study on the predictive ability of the decision tree, support vector machine and neuro-fuzzy models in landslide susceptibility mapping using GIS. *Computers and Geosciences, 51*, 350–365. https://doi.org/10.1016/j.cageo.2012.08.023

Pradhan, B., & Lee, S. (2010). Landslide susceptibility assessment and factor effect analysis: Backpropagation artificial neural networks and their comparison with frequency ratio and bivariate logistic regression modelling. *Environmental Modelling and Software, 25*(6), 747–759. https://doi.org/10.1016/j.envsoft.2009.10.016

Promper, C., Puissant, A., Malet, J. P., & Glade, T. (2014). Analysis of land cover changes in the past and the future as contribution to landslide risk scenarios. *Applied Geography, 53*, 11–19. https://doi.org/10.1016/j.apgeog.2014.05.020

Rabby, Y. W., Ishtiaque, A., & Rahman, M. S. (2020). Evaluating the effects of digital elevation models in landslide susceptibility mapping in rangamati district, Bangladesh. *Remote Sensing*. https://doi.org/10.3390/RS12172718

Raghuvanshi, T. K., Ibrahim, J., & Ayalew, D. Slope stability susceptibility evaluation parameter (SSEP) rating scheme—An approach for landslide hazard zonation. *Journal of African Earth Sciences, 99*(PA2), 595–612. https://doi.org/10.1016/j.jafrearsci.2014.05.004

Rawat, M. S., Uniyal, D. P., Dobhal, R., Joshi, V., Rawat, B. S., Bartwal, A., Singh, D., & Aswal, A. (2015). Study of landslide hazard zonation in Mandakini Valley, Rudraprayag district, Uttarakhand using remote sensing and GIS. *Current Science, 109*(1).

Riley, S. J., DeGloria, S. D., & Elliot, R. (1999). A terrain ruggedness index that qauntifies topographic heterogeneity. *Intermountain Journal of Sciences, 5*(1–4), 23–27.

Roy, J., & Saha, S. (2019). Landslide susceptibility mapping using knowledge driven statistical models in Darjeeling District, West Bengal, India. *Geoenvironmental Disasters*. https://doi.org/10.1186/s40677-019-0126-8

Saha, A., Pal, S. C., Chowdhuri, I., Chakrabortty, R., & Roy, P. (2022). Understanding the scale effects of topographical variables on landslide susceptibility mapping in Sikkim Himalaya using deep learning approaches. *Geocarto International, 37*(27), 17826–17852. https://doi.org/10.1080/10106049.2022.2136255

Saha, A. K., Gupta, R. P., & Arora, M. K. (2002). GIS-based Landslide Hazard Zonation in the Bhagirathi (Ganga) Valley, Himalayas. *International Journal of Remote Sensing, 23*(2), 357–369. https://doi.org/10.1080/01431160010014260

Sarkar, S., & Kanungo, D. P. (2004). An integrated approach for landslide susceptibility mapping using remote sensing and GIS. *Photogrammetric Engineering and Remote Sensing, 70*(5), 617–625. https://doi.org/10.14358/PERS.70.5.617

Sarkar, S., Kanungo, D. P., & Mehrotra, G. S. (1995). Landslide Hazard Zonation: A case study in Garhwal Himalaya, India. *Mountain Research and Development, 15*(4), 301–309.

Sarkar, S., Roy, A. K., & Martha, T. R. (2013). Landslide susceptibility assessment using Information Value Method in parts of the Darjeeling Himalayas. *Journal of the Geological Society of India, 82*(4), 351–362. https://doi.org/10.1007/s12594-013-0162-z

Sarma, C. P., Dey, A., & Krishna, A. M. (2020). Influence of digital elevation models on the simulation of rainfall-induced landslides in the hillslopes of Guwahati, India. *Engineering Geology*. https://doi.org/10.1016/j.enggeo.2020.105523

Schuster, R. L., & Fleming, R. W. (1986). Economic losses and fatalities due to landslides. *Bulletin of the Association of Engineering Geologists*. https://doi.org/10.2113/gseegeosci.xxiii.1.11

Schuster, R. L., & Highland, L. M. (2007). The third hans cloos lecture. Urban landslides: Socioeconomic impacts and overview of mitigative strategies. *Bulletin of Engineering Geology and the Environment, 66*(1), 1–27. https://doi.org/10.1007/s10064-006-0080-z

Shirzadi, A., Soliamani, K., Habibnejhad, M., Kavian, A., Chapi, K., Shahabi, H., Chen, W., Khosravi,K., Pham, B. T., Pradhan, B., Ahmad, A., Bin Ahmad, B., & Bui, D. T. (2018). Novel GIS based machine learning algorithms for shallow landslide susceptibility mapping. *Sensors (switzerland), 18*(11), 234. https://doi.org/10.3390/s18113777

Soria, D., Garibaldi, J. M., Ambrogi, F., Biganzoli, E. M., & Ellis, I. O. (2011). A 'non-parametric' version of the naive Bayes classifier. *Knowledge-Based Systems, 24*(6), 775–784. https://doi.org/10.1016/j.knosys.2011.02.014

Tan, Q., Wang, P., Hu, J., Zhou, P., Bai, M., & Hu, J. (2020). The application of multi-sensor target tracking and fusion technology to the comprehensive early warning information extraction of landslide multi-point monitoring data. *Measurement: Journal of the International Measurement Confederation, 166*, 108044. https://doi.org/10.1016/j.measurement.2020.108044

Tien Bui, D., Nguyen, Q. P., Hoang, N. D., & Klempe, H. (2017). A novel fuzzy K-nearest neighbor inference model with differential evolution for spatial prediction of rainfall-induced shallow landslides in a tropical hilly area using GIS. *Landslides, 14*(1), 1–17. https://doi.org/10.1007/s10346-016-0708-4

Tropeano, D., & Turconi, L. (2002). Using historical documents for landslide, debris flow and stream flood prevention. Applications in Northern Italy. *Natural Hazards, 31*(October 2004), 663–679.

van Beek, L. P. H., & van Asch, T. W. J. (2004). Regional assessment of the effects of land-use change on landslide hazard by means of physically based modelling. *Natural Hazards, 31*(1), 289–304. https://doi.org/10.1023/B:NHAZ.0000020267.39691.39

Xu, C., Xu, X., Shyu, J. B. H., Zheng, W., & Min, W. (2014). Landslides triggered by the 22 July 2013 Minxian-Zhangxian, China, Mw 5.9 earthquake: Inventory compiling and spatial distribution analysis. *Journal of Asian Earth Sciences, 92*(July 2013), 125–142. https://doi.org/10.1016/j.jseaes.2014.06.014

Zare, M., Pourghasemi, H. R., Vafakhah, M., & Pradhan, B. (2013). Landslide susceptibility mapping at Vaz Watershed (Iran) using an

artificial neural network model: A comparison between multilayer perceptron (MLP) and radial basic function (RBF) algorithms. *Arabian Journal of Geosciences, 6*(8), 2873–2888. https://doi.org/10.1007/s12517-012-0610-x

Zhao, X., & Chen, W. (2020). Optimization of computational intelligence models for landslide susceptibility evaluation. *Remote Sensing*. https://doi.org/10.3390/rs12142180